AMERICAN SOCIETY FOR MICROBIOLOGY | Journal of Virology

Diminished Innate Antiviral Response to Adenovirus Vectors in cGAS/STING-Deficient Mice Minimally Impacts Adaptive Immunity

Daniela Anghelina,* Eric Lam,* Erik Falck-Pedersen

Weill Cornell Medical College, Department of Microbiology and Immunology, Molecular Biology Graduate Program, New York, New York, USA

ABSTRACT

Infection by adenovirus, a nonenveloped DNA virus, induces antiviral innate and adaptive immune responses. Studies of transformed human and murine cell lines using short hairpin RNA (shRNA) knockdown strategies identified cyclic guanine adenine synthase (cGAS) as a pattern recognition receptor (PRR) that contributes to the antiadenovirus response. Here we demonstrate how the cGAS/STING cascade influences the antiviral innate and adaptive immune responses in a murine knockout model. Using knockout bone marrow-derived dendritic cells (BMDCs) and bone marrow-derived macrophages (BMMOs), we determined that cGAS and STING are essential to the induction of the antiadenovirus response in these antigen-presenting cells (APCs) *in vitro*. We next determined how the cGAS/STING cascade impacts the antiviral response following systemic administration of a recombinant adenovirus type 5 vector (rAd5V). Infection of cGAS$^{-/-}$ and STING$^{-/-}$ mice results in a compromised early antiviral innate response compared to that in wild-type (WT) controls: significantly lower levels of beta interferon (IFN-β) secretion, low levels of proinflammatory chemokine induction, and reduced levels of antiviral transcript induction in hepatic tissue. At 24 h postinfection, levels of viral DNA and reporter gene expression in the liver were similar in all strains. At 28 days postinfection, clearance of infected hepatocytes in cGAS or STING knockout mice was comparable to that in WT C57BL/6 mice. Levels of neutralizing anti-Ad5V antibody were modestly reduced in infected cGAS mice. These data support a dominant role for the cGAS/STING cascade in the early innate antiviral inflammatory response to adenovirus vectors. However, loss of the cGAS/STING pathway did not affect viral clearance, and cGAS deficiency had a modest influence on the magnitude of the antiviral humoral immune response to adenovirus infections.

IMPORTANCE

The detection of viral infection by host sentinel immune cells contributes to the activation of a complex and varied antiviral innate and adaptive immune response, which limits virus replication, spread, and susceptibility to infection. In this study, we have characterized how the cGAS/STING DNA-sensing cascade contributes to early detection of adenovirus infections. cGAS influences APC activation and early innate antiviral inflammatory immune responses, but adaptive immune pathways associated with virus clearance and anti-Ad antibody production were minimally influenced by the loss of the cGAS PRR signaling cascade.

Human adenoviruses (Ads) are a family of nonenveloped double-stranded DNA viruses that contribute to upper respiratory infections, epidemic conjunctivitis, and severe acute respiratory diseases in military recruits (1). Among the 57 serotypes of human adenoviruses, the group C type 2 and 5 adenoviruses are the most studied, providing a basic foundation for adenoviral mechanisms of transformation, viral gene expression, viral DNA replication, and virus entry. Replication-defective versions of adenovirus type 5 (Ad5) have been widely used as vectors for gene delivery, gene therapy, anticancer, and DNA vaccine applications. Infection by wild-type (WT) adenoviruses or replication-defective recombinant Ad5 vectors (rAd5Vs) stimulates an antiviral innate response that is followed by cellular and humoral antiviral immune responses.

Virus uptake by immune sentinel macrophages and dendritic cells (DCs) plays a pivotal role in determining the outcome of a viral infection. Macrophages contribute directly to viral clearance (2–4). Virus uptake by these cells triggers an antiviral response through the activation of pattern recognition receptors (PRRs) (5–9). Induction of beta interferon (IFN-β), a type I interferon, was established nearly 50 years ago as a dominant feature of the antiviral recognition response to adenovirus (10, 11). Adenovirus DNA (vDNA) was subsequently identified as a pathogen-associated molecular pattern (PAMP) that led to IFN-β induction (12). Using a variety of model systems, several PRRs, including Toll-like receptor 9 (TLR9), DAI, DDX41, p204 (IFI16), RNA polymerase III (Pol III), and cyclic adenine guanine synthase (cGAS), have been identified as DNA sensors that can lead to type I IFN expression (reviewed in references 13–15). Two general rAdV-responsive, IFN-β-inducing, DNA-sensing cascades have been identified: one is MyD88 dependent and the other is MyD88 independent (7). The TLR9/MyD88 cascade is activated by vDNA in plasmacytoid dendritic cells (pDCs) (7). This cascade signals through TRAF6 stimulation of interferon response factor 7 (IRF7), a transcription factor that binds a consensus IRF binding

Received 16 March 2016 **Accepted** 9 April 2016

Accepted manuscript posted online 13 April 2016

Citation Anghelina D, Lam E, Falck-Pedersen E. 2016. Diminished innate antiviral response to adenovirus vectors in cGAS/STING-deficient mice minimally impacts adaptive immunity. J Virol 90:5915–5927. doi:10.1128/JVI.00500-16.

Editor: G. McFadden, University of Florida

Address correspondence to Erik Falck-Pedersen, efalckp@med.cornell.edu.

* Present address: Daniela Anghelina, Hospital for Special Surgery, New York, New York, USA; Eric Lam, NYIT School of Osteopathic Medicine, Glen Head, New York, USA.

site, AANNGAAA, present in the IFN-β promoter (16–18). In conventional DCs or macrophages, adenovirus induction of IFN-β occurs through the activation of IRF3 by a MyD88-independent mechanism (6, 7, 19). Virus entry, endosomal escape, and exposure of vDNA to the cytosol are required for the activation of IRF3 (6). Presumably, vDNA is exposed to PRRs during the process of transport to the nucleus. In murine and human cell lines, cGAS (20, 21) has been identified as a vDNA PRR required for IFN-β induction following adenovirus infection of responsive cell lines (22, 23).

The mechanism for cGAS induction of IRF3 has been established through *in vitro* studies. Binding of DNA by cGAS induces protein conformational changes and homodimerization (24, 25). Dimerized cGAS synthesizes 2′-3′ cyclic guanine adenine monophosphate (cGAMP) (20, 26, 27), and cGAMP binds to the STING adaptor protein. Activation of STING results in migration from the endoplasmic reticulum to membrane vesicles associated with autophagosome proteins (28, 29). STING binds tank-binding kinase 1 (TBK1), and TBK1 undergoes phosphorylation (^{pSer172}TBK1) (30–32). The STING/TBK1 scaffold complex binds IRF3, presenting the C-terminal domain of IRF3 to TBK1 for phosphorylation (^{pSer396}IRF3) (31). ^{pSer396}IRF3 undergoes dimerization and translocation to the nucleus, where it engages the beta interferon promoter consensus IRF-binding site and contributes to the upregulation of beta interferon gene expression (33–36). Not all cells are equally equipped to carry out an efficient antiviral recognition response. Differences in virus entry and variable levels of either cGAS or STING impact the potency of the primary antiviral recognition response (22, 37).

Through the activation of IRF3 and the induction of IFN-β, the cGAS-induced antiviral cascade is amplified by autocrine and paracrine IFN-β activation of secondary signaling cascades (reviewed in reference 38). IFN-β binds to interferon receptor I (IFNRI) present on infected and uninfected cells. IFNRI activation mediates Tyk/Jak phosphorylation of STAT1 and STAT2, the formation of interferon-stimulated gene factor 3 (ISGF3), and the transcriptional activation of interferon-stimulated genes (ISGs) (39). Although IFN-β is a dominant feature of the antiviral secondary signaling response to rAd5V, other cytokines and chemokines (tumor necrosis factor alpha [TNF-α], interleukin-6 [IL-6], and IL-1) are also expressed following virus infection and make significant contributions to the antiviral response to rAdV. In cell line models, the antiviral response to rAdV is minimally a combination of two cell populations, naive uninfected cells that undergo simple paracrine cytokine stimulation and infected cells that have undergone both primary antiviral response signaling and secondary cytokine-induced autocrine signaling.

In vivo, several additional factors contribute to the initiation of both the innate and adaptive antiviral immune responses to rAdV (40). Following systemic administration of virus, rAd5 virions are exposed to diverse serum factors. Serum proteins such as factor X (41–43), native antibodies (3, 4, 44), or preexisting serotype-specific antibody (45) can bind virus and influence mechanisms contributing to virus uptake, transduction, localization, and intracellular signaling. How these interactions impact antiadenovirus responses has not been fully established. A second layer of complexity occurs by the varied population of cells that take up virus *in vivo* (i.e., neutrophils, macrophages, dendritic cells, endothelial cells, and hepatocytes). Depending on delivery and the availability of PRR/adaptor complexes, each cell type may initiate a unique antiviral response program. The *in vivo* antiviral response to adenovirus reflects the combined aggregate of cell-specific primary activation responses overlaid with cytokine/chemokine-mediated secondary signaling.

The antiviral response to rAdV matures with time. The early PRR innate response occurs rapidly at 0 to 6 h postinfection (p.i.) in the murine model, and by 24 h, the ISG transcript induction phase is in decline (46). At this point, the majority of systemically administered virus is cleared through innate mechanisms (47). Coincident with vector clearance, infected dendritic cells undergo maturation and migration to regional lymph nodes, where, through the presentation of viral antigens, they stimulate CD4 and CD8 T-cell activation against viral epitopes (48). In immunocompetent murine models, the presentation of virus-associated gene products by infected cells contributes to efficient elimination through T-cell-mediated cytolysis (49–51). Since DC maturation contributes to both T- and B-cell antigen-dependent selection, defects in antigen-presenting cell (APC) maturation may impact the antiviral adaptive immune response.

In this study, we have determined how the antiviral recognition response in APCs derived from cGAS and STING knockout (KO) mice compares to that in wild-type cells derived from C57BL/6 mice or from a negative-control IRF3$^{-/-}$ knockout strain. We extend our characterization of these knockout strains to assess how early innate antiviral signaling is altered in response to systemic administration of rAd5V and how these mutant mouse strains impact the hepatic clearance of rAdV and the production of antiadenovirus neutralizing antibody (NAb).

MATERIALS AND METHODS

Viruses. Ad5CiG and Ad5βGal were previously described (52, 53) and were grown on a large scale in HEK-293 cells according to standard protocols, purified through two rounds of CsCl gradient ultracentrifugation, and stored at −80°C in storage buffer (10 mM Tris, 2 mM $MgCl_2$, 4.0% sucrose [pH 7.5]). Virus particle numbers were quantified by spectrophotometric detection of intact virions at an optical density at 260 nm (OD_{260}) (10^{12} particles/OD_{260} unit).

Mice. Eight- to twelve-week-old male and female C57BL/6 and C57BL/6J-*Tmem173*^{gt}/J (STING KO) mice were obtained from Jackson Laboratories, cGAS$^{-/-}$ C57BL/6 mice were generously provided by H. Virgin, and IRF3$^{-/-}$ mice were generously provided by T. Taniguchi through Riken BRC.

Bone marrow-derived macrophages and dendritic cells. Bone marrow cells were extracted from the femurs and tibiae of mice. For bone marrow-derived macrophages (BMMOs), red cells were removed with a lysis solution (0.15 M NH_4Cl, 1 mM $KHCO_3$, 0.1 mM EDTA). Bone marrow cells were cultured in Dulbecco's modified Eagle's medium (DMEM) supplemented with 20% fetal bovine serum (FBS) and 25% supernatant derived from confluent L929 cells. On day 7, immature macrophages were collected. Bone marrow-derived dendritic cells (BMDCs) were differentiated in RPMI medium containing 10% FBS, 1% L-glutamine, and beta-mercaptoethanol (BME) in the presence of 20 ng/ml granulocyte-macrophage colony-stimulating factor (GM-CSF), as previously described (54). Briefly, bone marrow was harvested and plated into petri dishes at a density of 4×10^5 cells/ml, 10 ml/dish. At day 3, 10 ml of medium was added, and at days 6 and 8, 10 ml of medium was replenished. Immature, nonadherent BMDCs were gently harvested at day 10. The typical purity of each population was >90%, as determined by fluorescence-activated cell sorter (FACS) analysis of CD11b and CD11c surface markers, respectively.

Culture infections. BMMOs were harvested at day 7, BMDCs were harvested at day 10, and cells were plated at densities of 5×10^5 cells/ml in

12-well plates (Western blot and flow cytometry analyses) (5×10^5 cells/well) and 10^6 cells/ml in 6-well plates (for RNA extraction) (2.5×10^6 cells/well). Twenty-four hours after plating, cells were infected with Ad5CiG at 20,000 virus particles (vp)/cell and diluted in Opti-MEM. For Western blot analysis, cells were harvested at 2, 4, and 6 h p.i. Flow cytometry was performed at 24 h p.i., and RNA extraction was performed at 6 h p.i.

Animal infections. Mice were infected by intraorbital intravenous (i.v.) injections with 10^{11} vp/mouse of Ad5βGal diluted in DMEM. Mice were euthanized at 5 h, 24 h, and 28 days postinfection for liver and blood serum harvest. All experiments were performed in accordance with Weill Cornell Medical College IACUC protocols.

Antibodies, surface staining, and fixation. Antibodies were purchased from BioLegend (San Diego, CA). BMMOs and BMDCs were prepared from bone marrow as described above. For phenotypic analysis, cells were surface stained with the following monoclonal antibodies (MAbs): anti-CD11b allophycocyanin (APC) (catalog number 101212), anti-CD11c Pac Blue (catalog number 117322), anti-CD11c APC (catalog number 117310), anti-CD86 phycoerythrin (PE) (catalog number 105008), and anti-major histocompatibility complex class II (MHC-II) peridinin chlorophyll protein (PerCP)-Cy5.5 (catalog number 116416). After staining, washing, and fixation in 1% paraformaldehyde, cells were analyzed by using a FACSCanto flow cytometer (BD Biosciences). Data analysis was performed by using FlowJo software, and 12,000 events per sample were analyzed.

Western blot analysis. Whole-cell extracts were prepared by washing cells twice with ice-cold phosphate-buffered saline (PBS) and incubating them in lysis buffer (50 mM Tris [pH 7.5], 150 mM NaCl, 1 mM EDTA, 1% NP-40) with the addition of Phosphatase Inhibitor Cocktails 1 and 2 (catalog numbers P2850 and P5726; Sigma) and protease inhibitors (30 mM sodium fluoride, 1 mM phenylmethylsulfonyl fluoride [PMSF], 10 μg/ml aprotinin, 10 μg/ml leupeptin, 1 μg/ml pepstatin, 1 mM benzamidine) for 30 min at 4°C on a rocking platform before scraping and transferring cells to tubes. The lysates were cleared by centrifugation at 13,000 × *g* for 20 min at 4°C, and protein quantification was performed with the DC protein assay kit (Bio-Rad Laboratories).

For Western blot analysis, 20 μg total protein was separated by using standard 10% SDS-polyacrylamide gels and transferred onto polyvinylidene difluoride (PVDF) membranes (Immobilon P; Millipore). All blots were blocked in 5% skim milk in Tris-buffered saline (TBS) plus Tween (0.1%) at room temperature for 1 h. Phospho-IRF3 (Ser396) (catalog number 4947), phospho-STAT1 (58D6) (Tyr701) (catalog number 9167), beta-actin (catalog number 4967), total IRF3 (catalog number 4302), STING (catalog number 3337), TBK1 (catalog number 3503), phospho-NF-κB p65 (pNF-κB p65) (Ser536) (catalog number 3033), pTBK1 (Ser172) (catalog number 5483), green fluorescent protein (GFP) (catalog number 2956), and horseradish peroxidase (HRP)-linked anti-rabbit IgG (catalog number 7074) antibodies were obtained from Cell Signaling. Primary antibodies were used at a dilution of 1:2,000 to 1:3,000 in 5% bovine serum albumin (BSA)–TBS. The HRP-linked secondary antibody was diluted 1:4,000 in 5% milk–Tween–TBS. Detection was done with the Luminator Crescendo Western HRP substrate (Millipore).

SYBR green I RT-qPCR. Total cellular mRNA was isolated by using RNAzol reverse transcriptase (RT) (Molecular Research Center) according to the manufacturer's instructions. For RT quantitative PCR (RT-qPCR), a two-step protocol was employed: first, cDNA was synthesized from 2 μg total RNA in a volume of 20 μl by using random hexamer primers with the Maxima first-strand cDNA synthesis kit (Fermentas), and second, amplifications were carried out with a total volume of 15 μl by using the Maxima SYBR green/ROX qPCR master mix (Fermentas) in an Applied Biosystems Prism 7900H sequence detection system with SDS 2.1 software. Cycles consisted of an initial incubation step at 95°C for 10 min; 40 cycles at 95°C for 15 s, 60°C for 30 s, and 72°C for 30 s; and a melting-curve analysis cycle. Data acquisition was performed during the extension step. All determinations were performed in technical triplicate. Nontemplate and no-RT controls were run with every assay and had cycle threshold (C_T) values that were significantly higher than those of experimental samples or were not detected. The relative abundance of each mRNA was calculated by the $\Delta\Delta C_T$ method (55, 56), normalizing to Tata-binding protein (TBP) expression with standardization to one reference sample, as indicated. For comparisons between cell lines, or in late-stage virus infections, glyceraldehyde-3-phosphate dehydrogenase (GAPDH) was used as a normalization standard. Sequences of primers are available upon request.

SYBR green I qPCR of viral DNA. Liver fragments were Dounce homogenized in lysis buffer containing 10 mM NaCl, 10 mM Tris (pH 8.0), 10 mM EDTA (pH 8.0), and 0.5% SDS, followed by proteinase K digestion. Crude homogenates were cleared by double centrifugation. Total DNA was purified by using NaCl salting-out and ethanol precipitation protocols (57). Following DNA purification and resuspension in 100 μl H_2O, OD_{260} DNA concentrations were determined by using a NanoDrop instrument. Five nanograms of sample DNA in a final reaction mixture volume of 15 μl (Maxima SYBR green/ROX qPCR master mix [Fermentas] system) was used for each assay. Ad5 hexon and cellular control primers (IFN-β) were used to characterize each DNA sample. Normalization to the cellular genomic standard was used to derive the relative viral DNA yield/host genome. Assays were carried out with an Applied Biosystems Prism 7900H sequence detection system with SDS 2.1 software. Cycles consisted of an initial incubation step at 95°C for 10 min; 40 cycles at 95°C for 15 s, 60°C for 30 s, and 72°C for 30 s; and a melting-curve analysis cycle. Data acquisition was performed during the extension step. Data points represent the averages of results from biological and technical triplicates.

β-Gal assays. The Tropix Galacto-Star chemiluminescent reporter gene assay (catalog number T1012; Applied Biosystems) was used for β-galactosidase (β-Gal) detection in the livers of infected mice at 24 h and 28 days p.i., according to the manufacturer's protocol. Liver fragments were sonicated on ice for 20 s in 1 ml lysis buffer with PMSF. Homogenates were spun down twice at 13,000 rpm for 15 min. The supernatant was heat inactivated at 48°C for 1 h to neutralize endogenous β-galactosidase activity and spun down at 13,000 rpm for 15 min. The protein concentration was determined by a Bradford assay (58). Ten microliters of the supernatant per well was loaded into 96-well Immulon assay plates and incubated with 100 μl reaction buffer for 30 min at room temperature. The luminescence in each well was measured for 1 s. Each sample was loaded in triplicates, and data were averaged. The background given by the lysis buffer was subtracted, and results were expressed per microgram of liver protein.

Antibody neutralization assays. Mouse blood samples isolated at 28 days postinfection were left at room temperature for 15 min to allow clot formation and then centrifuged at 13,000 rpm for 10 min for serum separation. Mouse serum was immediately flash frozen and thawed when used for biological assays. Briefly, serum neutralization assays were carried out as follows. HeLa cells were plated out at 2.5×10^4 cells/well in 96-well plates 24 h prior to infection. On the following day, serum was thawed, and 1:4 serial dilutions in DMEM were generated for each serum sample. Ad5βGal, diluted in DMEM for a final delivery of 10^3 particles/cell, was incubated with a serum dilution (technical triplicates for each sample) for 1 h at 37°C. Following virus/serum incubation, the mixture was incubated with HeLa cells for 30 min at 37°C. Medium was removed, and cells were washed with fresh medium and incubated in 100 μl fresh medium for 24 h. At 24 h p.i., plates were spun down at 2,000 rpm for 5 min, and medium was removed. Cell lysates were harvested in a volume of 100 μl lysis buffer. Ten microliters of the supernatant was applied for a Tropix Galacto-Star activity assay as described above. The background generated by the lysis buffer was subtracted from the result for each assay point, and results were expressed as luminescence units.

Cytokine and chemokine multiplex assays. Mouse serum derived from blood samples as described above was harvested at the indicated times and stored at −80°C until it was evaluated in cytokine assays. Serum was centrifuged for 15 min at 13,000 rpm to remove any residual cells or

debris and then evaluated for cytokine secretion with Meso Scale Discovery (MSD) (Rockville, MD) technology using a mouse proinflammatory 7-plex tissue culture kit (catalog number K15012B-1). Kits were run according to the manufacturer's instructions. Samples were run in duplicate, at the Weill Cornell Medical School CTSC facility, by using Meso Scale Discovery Sector Imager 2400 (SI2400).

ELISA. Mouse IFN-β was measured by using a mouse IFN-β (PBL Interferon Source) enzyme-linked immunosorbent assay (ELISA) kit (catalog number 42400; R&D Systems). Serum from mice was obtained as described above and stored at −80°C until it was evaluated for cytokine secretion. Kits were run according to the manufacturer's instructions. The absorbance at 450 nm was read within 5 min after the addition of the stop solution. Each sample was assayed as a technical duplicate.

Statistical analysis. Data were expressed as means ± standard errors of the means. Statistical analysis was performed with Student's *t* test. A P value of <0.05 was considered significant.

RESULTS

The antiviral response to rAdV is compromised in cGAS- and STING-deficient murine BMMOs. Short hairpin RNA (shRNA) knockdown assays targeting cGAS, STING, and TBK1 were previously used to identify these proteins as components of the anti-adenovirus DNA recognition response in both human and murine cell lines (23, 37). To establish the essentiality of STING to adenovirus-induced recognition responses in primary murine macrophages, bone marrow-derived CD11b$^+$ macrophages were isolated from WT C57BL/6 and Goldenticket mice containing a null STING allele (59). As a negative control, BMMOs were also isolated from C57BL/6 IRF3 knockout (IRF3$^{-/-}$) mice. BMMOs from each strain were infected with first-generation (E1$^-$/E3$^-$) replication-defective Ad5CiG (cytomegalovirus [CMV]-driven chloramphenicol acetyltransferase internal ribosome entry site [IRES] GFP [CATiresGFP] reporter gene cassette) (2×10^4 vp/cell). Cell protein lysates were harvested over a 6-h time course. Western blot analysis of lysates from WT BMMOs revealed a time-dependent increase in the phosphorylation of TBK1 and IRF3 (Fig. 1A). TBK1 and IRF3 are primary response markers, which undergo activation as a direct consequence of viral DNA recognition by the cGAS/STING PRR machinery. In contrast to WT BMMOs, infection of STING$^{-/-}$ BMMOs did not result in the phosphorylation of TBK1 or IRF3. Lysates generated by infection of BMMOs from negative-control IRF3$^{-/-}$ mice indicated that the primary DNA recognition cascade was intact (enhanced phosphorylation of TBK1), which is consistent with IRF3 being a downstream substrate for TBK1.

IRF3 phosphorylation, dimerization, and translocation to the nucleus are required for transcriptional activation of IFN-β. IFN-β expression and secretion contribute to the secondary antiviral signaling response. Activation of type I IFN receptor (IFNRI) triggers the phosphorylation of STAT1; therefore, the induction of ^{pTyr701}STAT1 provides a marker for the secondary antiviral signaling response. Lysates harvested from infected STING$^{-/-}$ or IRF3$^{-/-}$ BMMOs were severely restricted in the phosphorylation of STAT1 compared to BMMOs from WT mice. Our data indicate that both primary and secondary signaling responses to rAdV were compromised in STING-deficient and IRF3$^{-/-}$ BMMOs.

As indicated above, the combination of primary and secondary antiviral signaling leads to transcriptional activation of proinflammatory genes and ISGs. To determine the influence of the STING deficiency on antiviral gene induction, total RNA harvested at 6 h postinfection was characterized by a two-step RT-qPCR assay (Fig. 1B). Levels in all samples were normalized to the level of TBP by using the $\Delta\Delta C_T$ method, where the value for mock WT sample 1 was set as an arbitrary unit of 100. As a quantitative reference, the unnormalized average C_T for each mock WT primer pair is indicated above the expression bar (Δ1 log ~3 C_T, and C_Ts of >30 indicate relatively low-abundance transcripts). Transcripts corresponding to IFN-β, ISG15, ISG54, VIP, CXCL9, TNF-α, IL-1β, and IL-6 were strongly induced following infection of BMMOs from WT mice. In contrast, induction of these transcripts was not observed following infection of STING$^{-/-}$ or IRF3$^{-/-}$ BMMOs. We also found that basal levels of several transcripts (ISG15, ISG54, viperin (VIP), TNF-α, and IL-1β) were significantly reduced in BMMOs from both knockout strains. Macrophage maturation following virus uptake results in the upregulation of the costimulatory protein CD86 at 24 to 48 h postinfection (Fig. 1C and D). CD86 surface expression levels following infection of STING$^{-/-}$ or IRF3$^{-/-}$ BMMOs were significantly lower than levels found with WT BMMOs. Based on these criteria, primary and secondary signaling markers, induction of antiviral gene expression, and upregulation of costimulatory CD86, BMMOs from STING-deficient mice were essentially nonresponsive to rAdV infection.

We next obtained BMMOs from cGAS (MB21D1) knockout mice (60), allowing us to confirm the role of cGAS in the antiviral response to rAdV. cGAS$^{-/-}$ BMMOs infected with rAd5CiG were harvested over a 6-h time course for protein lysates or at 24 h postinfection to assess CD86 surface expression. Western blot analysis of cGAS BMMO-derived protein lysates revealed a complete lack of primary and secondary activation events (pTBK1, pIRF3, and pSTAT1) in cGAS KO compared to WT infections (Fig. 2A). Using CD86 upregulation as a maturation marker, cGAS BMMOs failed to mature in response to rAdV infection (Fig. 2B). These experiments demonstrate that the cGAS/STING DNA sensor complex functions as the dominant PRR pathway for rAdV infection of murine BMMOs.

cGAS and STING deficiencies limit the antiadenovirus response in CD11c$^+$ bone marrow-derived dendritic cells. While macrophages contribute to virus clearance through phagocytic elimination of virus and secretion of inflammatory chemokines, virus uptake by dendritic cells (DCs) results in the maturation of DCs into highly efficient professional antigen-presenting cells (APCs). Bone marrow progenitor cells grown in the presence of GM-CSF differentiate into a CD11c$^+$ immature dendritic cell type (BMDCs). Using cultures of GM-CSF-differentiated BMDCs isolated from WT, STING$^{-/-}$, IRF3$^{-/-}$, and cGAS$^{-/-}$ mice, we determined how these mutations influenced the BMDC antiviral response. Day 10 BMDCs were infected with 2×10^4 Ad5CiG vp/cell, and protein lysates were harvested at the indicated times over a 6-h time course (Fig. 3A). Western analysis of WT BMDC protein lysates indicated that IRF3, TBK1, and STAT1 are phosphorylated in a time-dependent manner following exposure to rAd5CiG. In contrast, analysis of lysates from infected cGAS$^{-/-}$ and STING$^{-/-}$ BMDCs revealed levels of pIRF3, pTBK1, and pSTAT1 that were similar to those in uninfected mock samples. Consistent with observations made in BMMOs, infection of IRF3$^{-/-}$ BMDCs resulted in the production of pTBK1 in a time-dependent manner. Additionally, low levels of pSTAT1 were present in infected IRF3$^{-/-}$ lysates. These data indicate that primary and secondary antiviral signaling responses were compromised in cGAS$^{-/-}$ and STING$^{-/-}$ BMDCs.

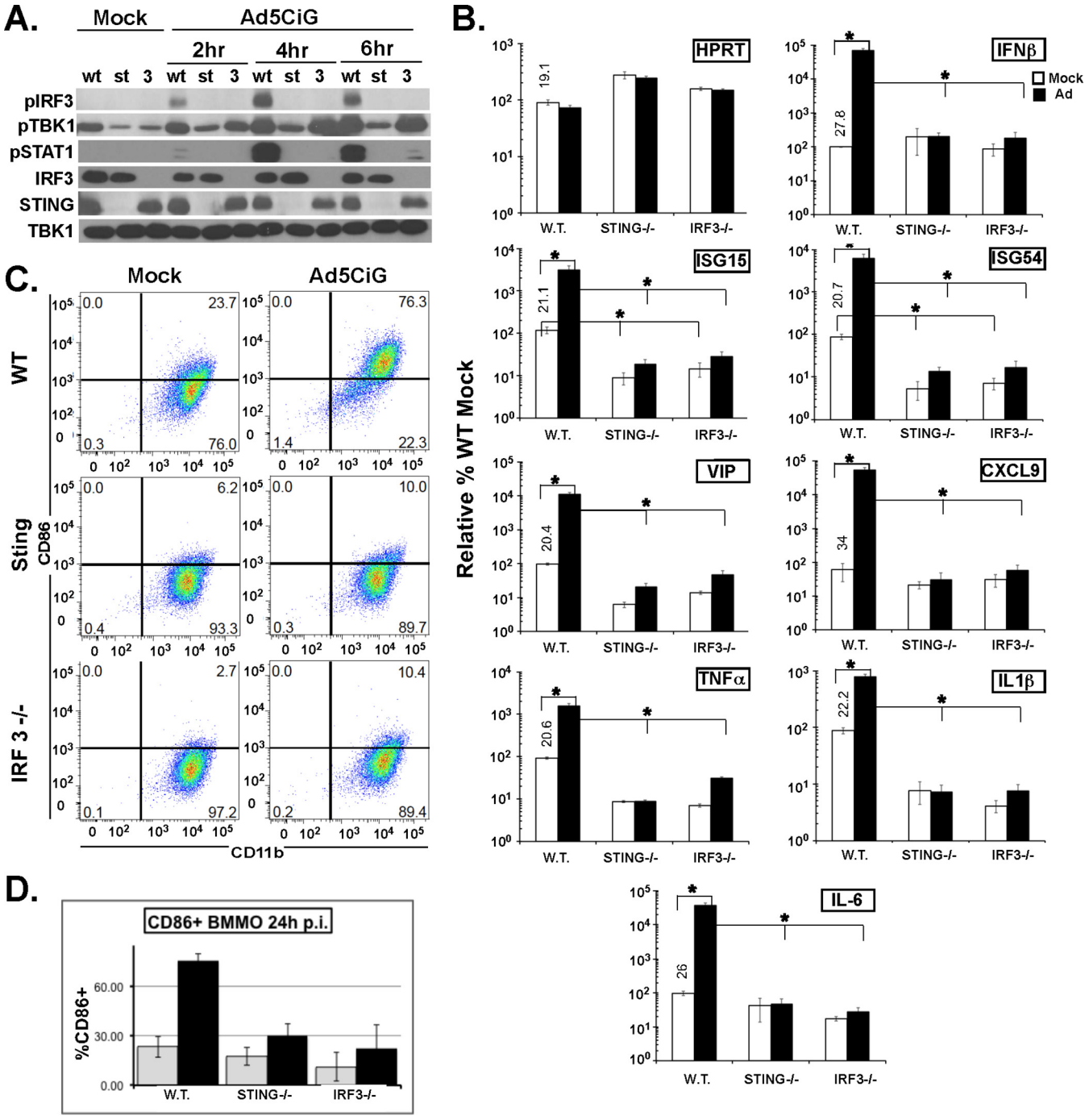

FIG 1 Characterization of the antiviral innate response to Ad5CiG infection in wild-type, STING$^{-/-}$, and IRF3$^{-/-}$ bone marrow-derived macrophages. (A) Western blot analysis of lysates harvested 2, 4, or 6 h after mock or Ad5CiG infection of wild-type (wt), STING$^{-/-}$ (st), and IRF3$^{-/-}$ (3) BMMOs with the indicated antibodies. (B) Two-step RT-qPCR of mRNA isolated from wild-type, STING$^{-/-}$, and IRF3$^{-/-}$ BMMOs. PCR primers correspond to hypoxanthine phosphoribosyltransferase (HPRT), IFN-β, ISG15, ISG54, VIP, CXCL9, TNF-α, IL-1β, and IL-6. Values for all samples were normalized to TBP values by using the $\Delta\Delta C_T$ method as described in Materials and Methods; mock scramble sample 1 was assigned an arbitrary value of 100. The unnormalized average C_T value for mock-treated WT samples is shown above the bar. All RT-qPCR assays included biological triplicates as well as technical triplicates for each sample. Statistical analysis was performed with Student's *t* test. A *P* value of <0.05 (*) was considered significant. (C) FACS analysis of bone marrow-derived macrophages after Ad5CiG infection. Cells were infected with 20,000 vp/cell of Ad5CiG and harvested at 24 h p.i. for FACS analysis after staining with anti-CD11b and anti-CD86 antibodies. (D) Frequencies of CD11b$^+$ CD86$^+$ cells within total cells analyzed. Data represent the averages of results from 3 experiments.

We next harvested total RNA from mock- or rAdV-infected BMDCs at 6 h postinfection. Two-step RT-qPCR was carried on all RNA samples as described above. The first observation taken from the RT-qPCR assay (Fig. 3B) was that transcript induction in each of the knockout strains was significantly compromised compared to that in infected WT BMDCs. Transcripts corresponding to IFN-β, ISGs, and proinflammatory transcripts were all impacted by these mutations. The IL-1β transcript was not apprecia-

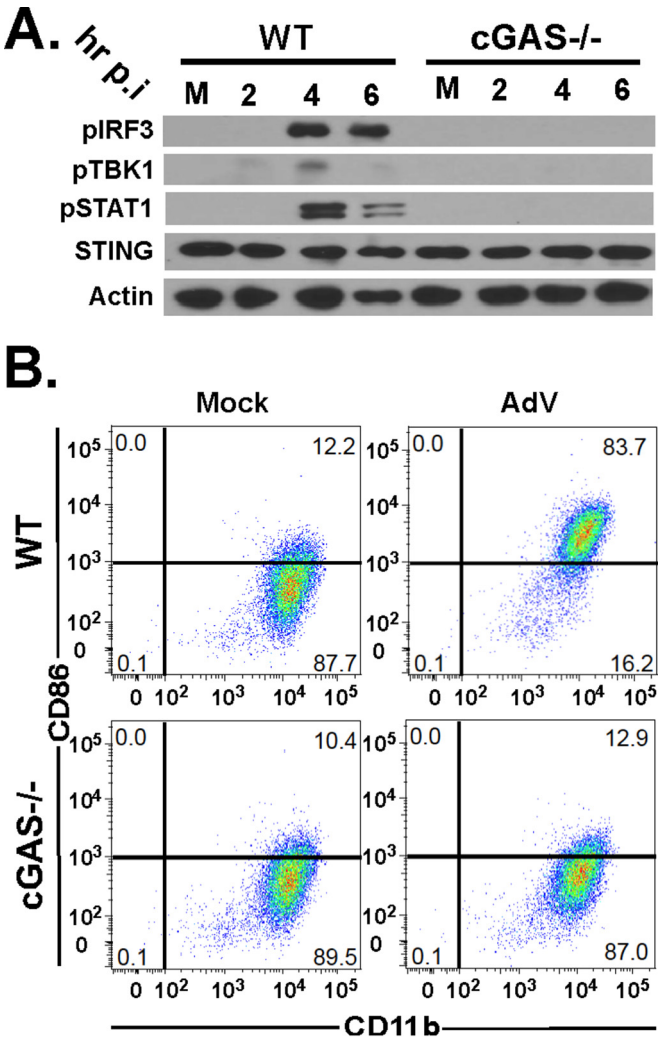

FIG 2 Characterization of the antiviral innate response to Ad5CiG infection of cGAS$^{-/-}$ bone marrow-derived macrophages. (A) Western blot analysis of lysates harvested 2, 4, or 6 h after mock (M) or Ad5CiG infection of wild-type and cGAS$^{-/-}$ BMMOs with the indicated antibodies. (B) FACS analysis of bone-marrow derived macrophages from cGAS$^{-/-}$ mice after Ad5CiG infection. Cells were infected with 20,000 vp/cell of Ad5CiG, harvested at 24 h p.i., and assayed by FACS analysis after staining with anti-CD11b and anti-CD86 antibodies. Dot plots are representative of results from 3 independent experiments (*, $P < 0.05$, as determined by a *t* test).

bly induced by rAd5CiG infection of WT BMDCs. A second observation taken from these assays was the existence of strain- and transcript-specific induction trends. For each strain, in comparisons between mock- and rAdV-treated samples, there were examples of low-level but significant transcript induction (notably with cGAS ISGs). The final observation taken from the RT-qPCR assay of BMDCs was that we did not find significant differences in basal levels of any ISG. Of note, low-level induction of IFN-β mRNA following infection of IRF3$^{-/-}$ BMDCs was observed, which is consistent with the low level of pSTAT1 observed in the BMDC Western analysis of protein lysates (Fig. 3A).

Upregulation of costimulatory markers is an important functional measurement of BMDC maturation in response to pathogen activation. BMDCs at 24 h postinfection were analyzed by flow cytometry for increased CD86 surface expression levels for each knockout strain (Fig. 3C and D). Consistent with compromised primary and secondary signaling, levels of CD86 surface expression from cGAS- or STING-deficient BMDCs exposed to rAd5CiG were at mock-infected levels. Therefore, at the levels of primary and secondary signaling, induction of antiviral transcripts, and upregulation of costimulatory molecules, we have established that the cGAS/STING DNA-sensing cascade is a critical component of the antiviral recognition response in primary murine BMDCs. We note that in BMMOs, these mutations resulted in an essentially nonresponsive anti-rAdV phenotype, while in BMDCs, the antiviral responses were severely compromised but not completely eliminated.

cGAS and STING deficiencies impact chemokine induction following intravenous administration of rAd5βGal. In the murine systemic infection model, administration of rAdV exposes virus to serum factors, including native antibody and factor X, which bind virus. The vast majority of virus localizes to the liver, where a heterogeneous population of cells, including hepatocytes, endothelial cells, macrophages (Kupffer cells), and dendritic cells, is exposed to rAdV. To determine the role of cGAS and STING in the *in vivo* antiviral recognition response, intravenous administration of 10^{11} rAd5βGal particles per mouse was carried out for each mouse strain. Mice were euthanized at 5 h postinfection for tissue and serum harvest ($n = 6$ to 9 mice/strain). We first characterized liver protein lysates for the activation of the IRF3 primary response marker and found that levels of pIRF3 from WT lysates were below detectable limits (Fig. 4A). From our experience, murine hepatocyte cell lines are nonresponsive to rAdV due to a lack of cGAS/STING expression (37). Hepatocytes make up the majority of the liver cell mass; therefore, the nonresponsive pool of cells may dilute and obscure the signal derived from responsive cells. When screening for the IFN secondary response marker pSTAT1, we found detectable induction of pSTAT1 in liver lysates from infected WT mice, whereas lysates from STING$^{-/-}$ mice had lower basal and induced levels of pSTAT1. The data from Western analysis imply that a low level of interferon expression occurred following infection of WT mice, which was compromised in knockout mice. An IFN-β ELISA was employed to directly quantitate serum IFN-β levels in all strains at 5 h postinfection ($n = 6$ mice/strain) (Fig. 4B). Serum IFN-β levels from mock-treated mice (WT and each knockout strain) were uniformly below the limit of detection (LOD) for the ELISA. A significant level of IFN-β was detected in serum from infected WT mice. Serum levels of IFN-β from all infected knockout mice were found to be statistically indistinguishable from those of mock-treated serum samples.

To assess the impact of cGAS/STING cascade deficiencies on rAdV-induced secretion of proinflammatory chemokines and cytokines, a mouse proinflammatory multiplex strip serum assay was carried out (which detects TNF-α, IL-6, CXCL1/KC, IL-10, IL-1β, IFN-γ, and IL-12p70). Data are presented for both mock- and rAd5βGal-treated mice ($n = 6$ mice/strain) at 5 h p.i.(Fig. 4C). Infection of WT mice resulted in elevated serum levels of TNF-α, IL-6, KC, and IL-10 compared to those in mock-infected mice. Significant changes in IL-1β and IL-12p70 levels were not detected. rAd5βGal infection of knockout strains generated significantly lower levels of serum TNF-α, IL-6, and IL-10 than did rAd5βGal infection of WT mice. Levels of both KC and IFN-γ were trending down, but differences were not statistically significant. Furthermore, we found diminished basal levels of several cytokines in untreated IRF3$^{-/-}$ and cGAS$^{-/-}$ mice. Diminished

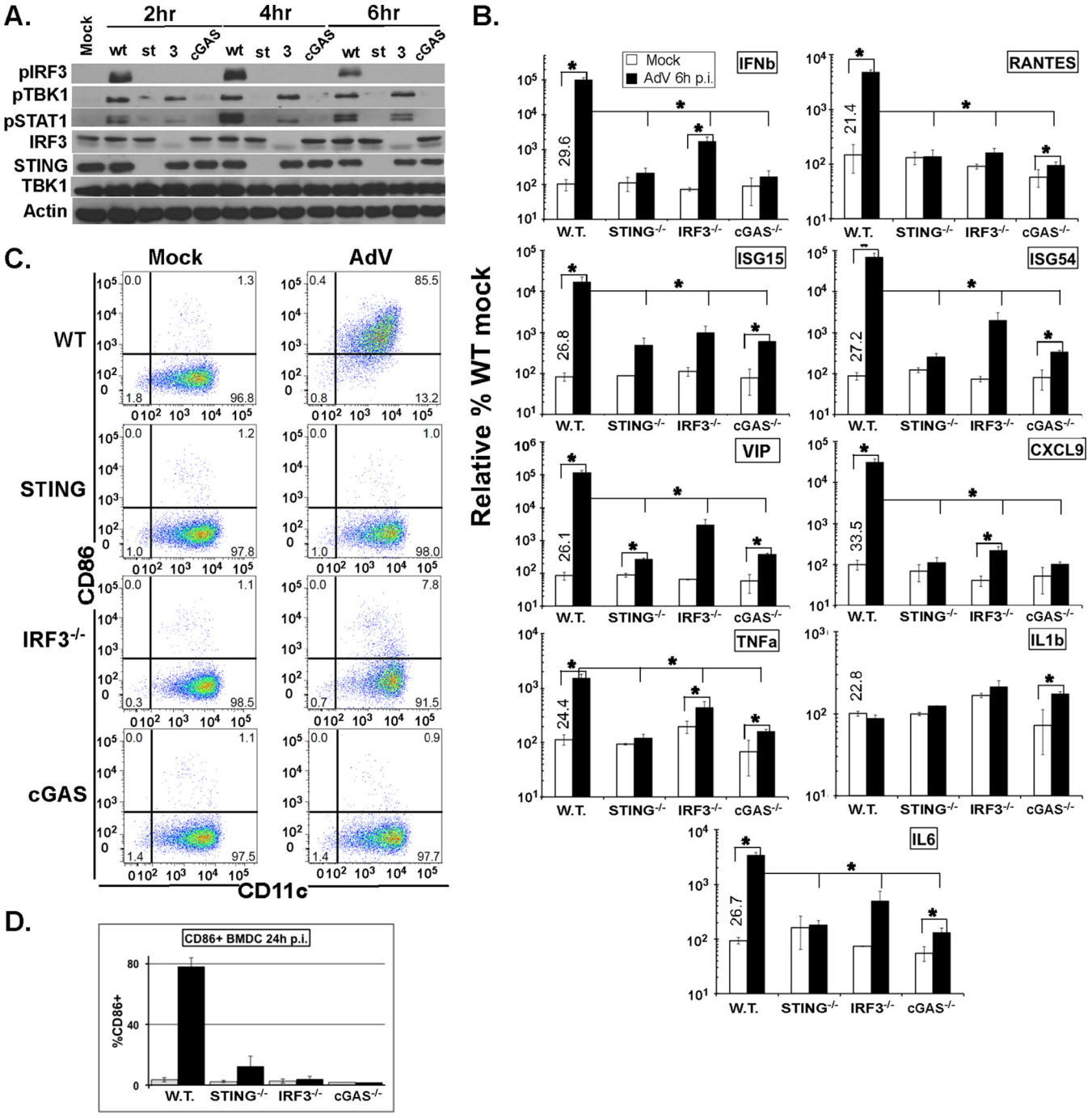

FIG 3 Characterization of the antiviral innate response to Ad5CiG infection in cGAS$^{-/-}$, STING$^{-/-}$, and IRF3$^{-/-}$ bone marrow-derived dendritic cells. (A) Western blot analysis of lysates harvested 2, 4, or 6 h after Ad5CiG infection of wild-type (wt), STING$^{-/-}$ (st), IRF3$^{-/-}$ (3), and cGAS$^{-/-}$ (cGAS) BMDCs with the indicated antibodies. A mock-treated sample from wild-type BMDCs harvested at 6 h is included. (B) Two-step RT-qPCR of mRNA isolated from wild-type, STING$^{-/-}$, IRF3$^{-/-}$, and cGAS$^{-/-}$ BMDCs. PCR primers correspond to IFN-β, RANTES, ISG15, ISG54, VIP, CXCL9, TNF-α, IL-1β, and IL-6. Values for samples were normalized to TBP values with the $\Delta\Delta C_T$ method. The unnormalized average C_T value for WT mock-treated samples is shown above the bar. A P value of <0.05 (*) was considered significant. (C) FACS analysis of bone marrow-derived dendritic cells after Ad5CiG infection. Cells were infected with 20,000 vp/cell of Ad5CiG, harvested at 24 h p.i., and assayed by FACS analysis after staining with anti-CD11c and anti-CD86 antibodies. (D) Frequencies of CD11c$^+$ CD86$^+$ cells within total cells analyzed. Data represent the averages of results from 3 experiments.

basal level of cytokines contributed to the identification of strain-specific instances of cytokine induction following rAd5βGal infection of knockout mice. Overall, these data indicate that cytokine levels are reduced in knockout strains, but a residual low-level antiviral cytokine induction response persists.

RT-qPCR analysis of 5- and 24-h antiviral response transcripts reveals an important role for the cGAS/STING pathway in activation of antiadenovirus responses *in vivo*. Data indicate that antiviral signaling cascades are compromised in cGAS, STING, and IRF3 knockout mice. To determine how these defi-

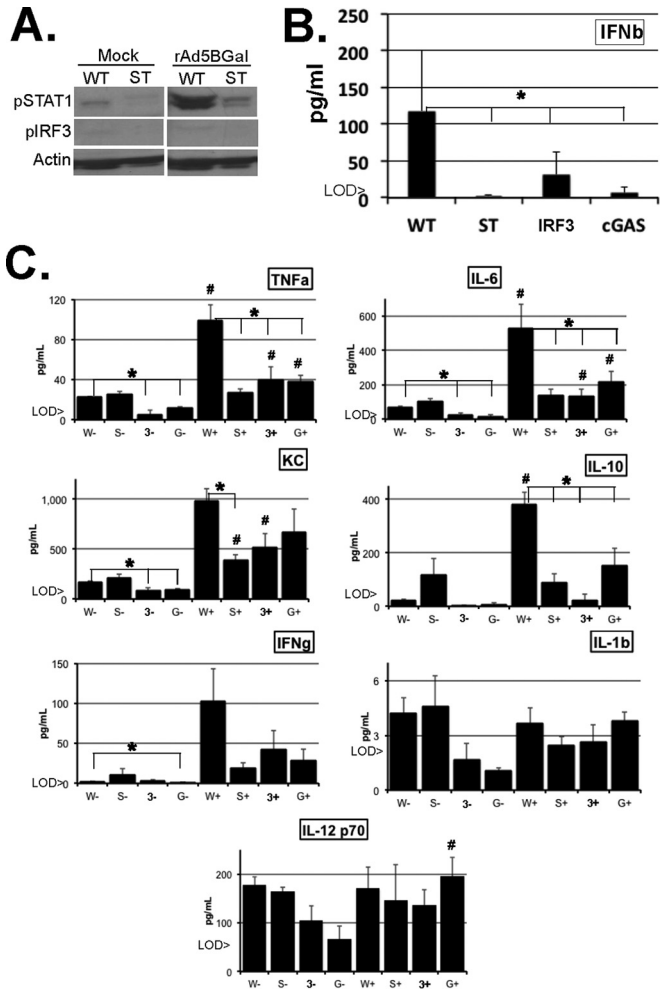

FIG 4 Characterization of the *in vivo* response to Ad5βGal infection in cGAS/STING cascade-deficient mice at 5 h postinfection. Mice were infected by i.v. administration of 10^{11} vp Ad5βGal/mouse. Mice were euthanized at 5 h postinfection for serum and tissue harvest. (A) Western blot analysis of liver homogenates 5 h after Ad5CiG infection of wild-type (WT) and STING$^{-/-}$ (ST) mice with the indicated antibodies. (B) Serum levels of IFN-β determined by an ELISA at 5 h postinfection. Levels of IFN-β in all mock-treated mice were uniformly below limits of detection. (C) Serum levels of TNF-α, IL-6, KC, IL-10, IFN-γ, IL-1β, and IL-12p70 were determined by a multiplex assay at 5 h p.i. Six mice were analyzed per strain, in 2 different experiments (*, $P < 0.05$, as determined by a *t* test) (# denotes comparison to the corresponding mock control).

ciencies influence the transcriptional induction of antiviral response transcripts, total liver RNA was isolated from mock- or rAd5βGal-infected mice at 5 and 24 h postinfection and used in a two-step RT-qPCR assay with the indicated primer pairs (Fig. 5). Exposure of WT mice to rAd5βGal resulted in ~2-log increases in IFN-β transcript and interferon-stimulated gene transcript levels corresponding to ISG15, ISG54, VIP, and CXCL9 at 5 h postinfection. Proinflammatory transcripts corresponding to TNF-α and IL-6 were significantly induced, whereas IL-1β was not. Levels of each transcript had declined by 24 h postinfection, with CXCL9 being the sole exception.

RT-qPCR analysis of total liver RNA from knockout strains at 5 h postinfection revealed significantly lower levels of the IFN-β transcript, which were similar to those in mock-treated mice (Fig. 5). For all strains, levels of IFN-β in mock-treated mice were extremely low and not significantly different from those for a no-RT control. Consistent with diminished levels of IFN-β and IFN-β transcripts (Fig. 4B and 5, respectively), rAdV-induced ISG and proinflammatory transcript levels from rAd5βGal-infected knockout strains were significantly lower than the levels observed for their WT counterparts, with the exception of CXCL9 (which was trending downward). Several additional observations were made from these assays. Basal levels of ISG15, ISG54, and VIP were diminished in IRF3 knockout samples but not in cGAS and STING knockout mice (in comparison to levels in mock-treated WT mice). It is apparent that in spite of the diminished levels of induced transcripts, there is persistent low-level induction of ISG15 and CXCL9 following Ad infection of knockout strains. Furthermore, ISG15 and CXCL9 were the only inducible transcripts whose levels were largely maintained above background levels at 24 h postinfection for all strains. At 24 h postinfection, levels of IFN-β, ISG54, VIG1, IL-6, and TNF-α were trending toward levels with mock treatment. Overall, these data strongly indicate that the cGAS/STING DNA-sensing cascade plays a major role in rAdV activation of innate antiviral responses *in vivo*.

cGAS/STING cascade deficiencies minimally impact virus clearance and the humoral immune response to rAdV. Following systemic rAdV infection, the vast majority of virus is cleared through phagocytic uptake by macrophages and neutrophils. Hepatocyte uptake of rAdV and ensuing vector transgene expression serve as a marker for the persistence of virus-infected cells in immunocompetent or compromised mouse models. Based on our observations that cGAS/STING DNA sensing of rAdV makes a major contribution to the early innate antiviral response *in vitro* and *in vivo*, we asked if mice deficient in the cGAS/STING cascade demonstrate a compromised ability to clear virus-infected cells. Administration of 10^{11} rAd5βGal vp/mouse for each strain ($n = 6$ to 9/strain/harvest time point, as described above) was followed by tissue harvest on day 1 or day 28 postinfection.

Transgene expression levels over 28 days are not significantly affected by cGAS or STING knockouts. As described in Materials and Methods, liver segments were homogenized and clarified by centrifugation for use in a Tropix Galacto-Star chemiluminescent β-Gal reporter gene expression assay and compared to strain-specific mock-infected lysates (Fig. 6A). At 1 day postinfection, levels of β-Gal expression from WT and mutant strains (STING$^{-/-}$, IRF3$^{-/-}$, and cGAS$^{-/-}$) were equally elevated (~3 logs) compared to those in mock-treated lysates. Under these experimental conditions, cGAS DNA-sensing cascade deficiencies did not result in significant differences in Ad-mediated liver transgene expression. In comparison to the levels of β-Gal expression at 1 day postinfection, liver homogenates from infected mice on day 28 postinfection revealed a significant loss of β-Gal expression for all mouse strains. We found no statistical difference between WT mice and each of the knockout strains. These data argue that clearance of virus-infected cells was not influenced by deficiencies of cGAS/STING DNA-sensing cascade components.

Viral DNA clearance is not diminished by cGAS or STING knockouts over a 28-day time course. Liver DNA was harvested from mock-infected mice and infected mice at 1 day and 28 days postinfection for quantitative PCR of viral DNA. qPCR of persistent viral DNA provides a reporter gene-independent assay for quantifying rAd5βGal and vDNA persistence. Five nanograms of total DNA from each liver sample ($n = 6$ mice/strain/time point)

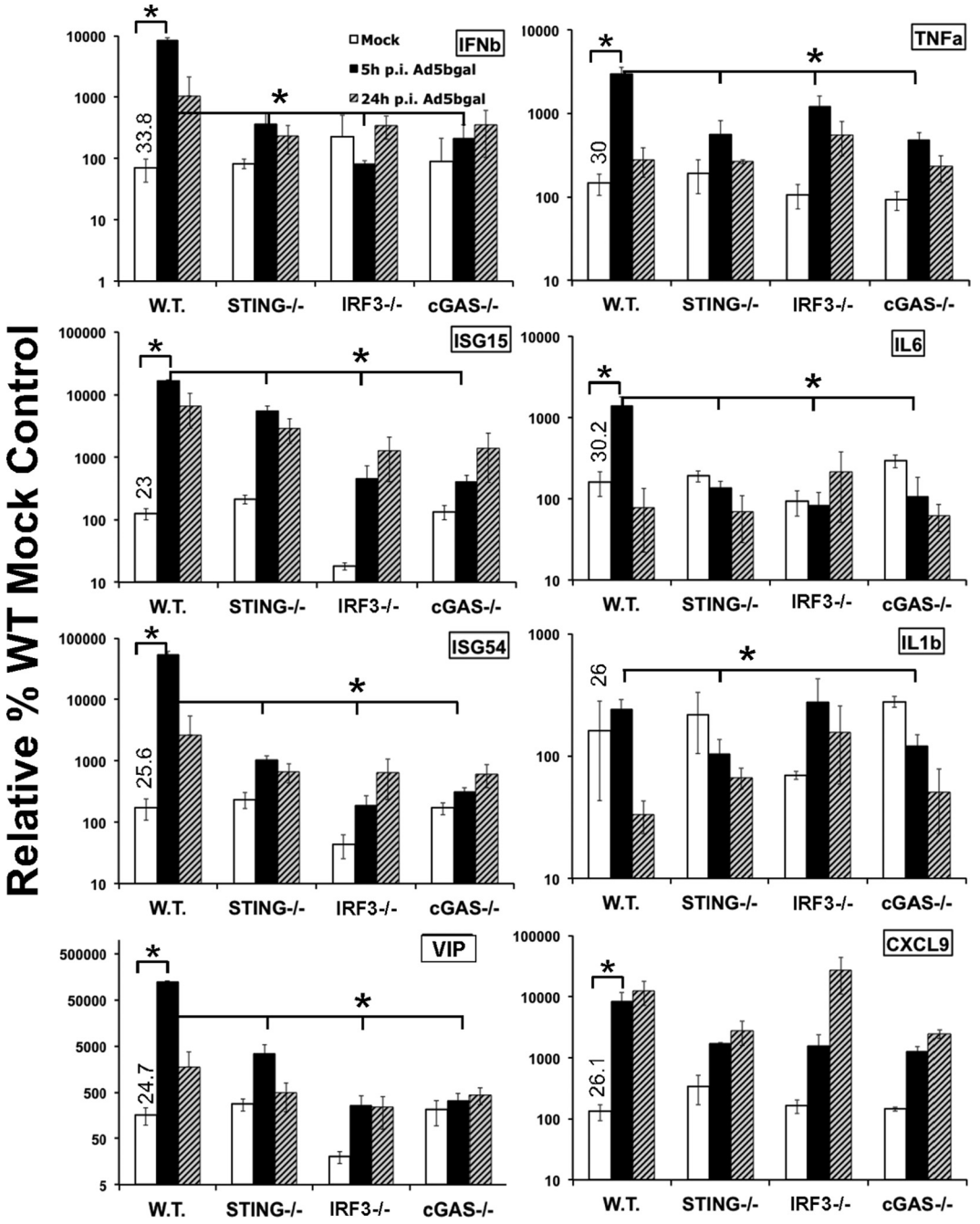

FIG 5 *In vivo* antiviral response to Ad5βGal infection as determined by RT-qPCR analysis of liver RNA from WT, STING$^{-/-}$, IRF3$^{-/-}$, and cGAS$^{-/-}$ mice harvested at 5 or 24 h p.i. Wild-type or KO animals were injected with PBS (mock) or Ad5βGal, as described in the text, and liver tissue was harvested at the indicated times and processed as described in Materials and Methods to obtain mRNA. mRNA from each sample was used in a two-step RT-qPCR assay with primer pairs corresponding to IFN-β, ISG15, ISG54, TNF-α, IL-6, IL-1β, VIP, and CXCL9. The unnormalized average C_T for WT mock-treated samples is shown above the bar. Values for samples were normalized to TBP values by using the $\Delta\Delta C_T$ method. A *P* value of <0.05 (*)was considered significant.

was used in a standard qPCR assay (see Materials and Methods), using an Ad5 hexon-specific primer pair with normalization to the value for a cellular IFN-β genomic control using the $\Delta\Delta C_T$ method. An infected WT sample from day 28 was arbitrarily assigned a relative vDNA expression value of 1 as a unit standard for all samples. Mock-infected samples from each strain resulted in no detection of rAd5βGal, as expected (Fig. 6B). For each sample derived from a 24-h total DNA harvest, we found no statistically significant differences in rAd5 hexon PCR products between each mouse strain. These data are in agreement with the observations made in transgene expression assays. Levels of viral DNA and transgene expression were similar in WT and cGAS/STING-deficient mice at 24 h postinfection.

In agreement with data from the β-Gal expression assays, levels of vDNA isolated from livers at 28 days postinfection were equally reduced for all strains. In comparison to mock-treated samples,

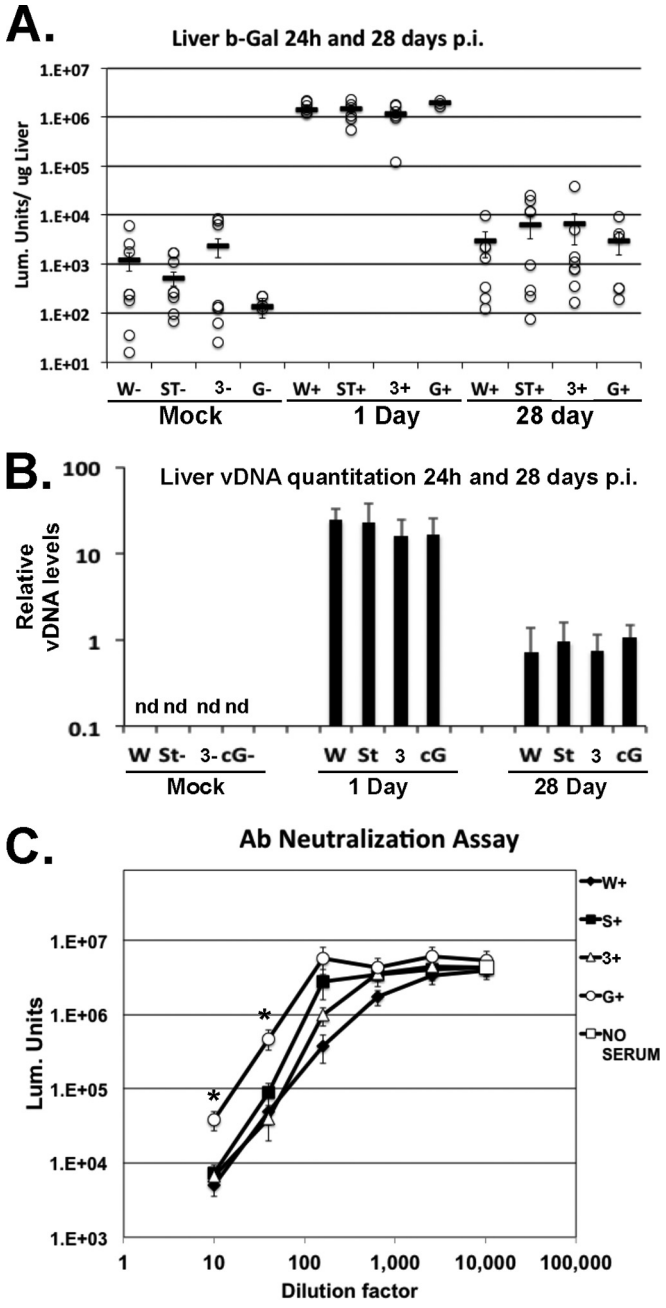

FIG 6 Impact of cGAS/STING/IRF3 KO mutations on virus clearance and the antiviral humoral immune response to Ad5βGal infection. (A) *In vivo* viral clearance, as determined by β-galactosidase activity in the livers of infected mice at 24 h and 28 days p.i. Liver fragments were sonicated, and β-Gal activity in the liver lysate was determined as described in Materials and Methods. Results are expressed in luminescence units per microgram of liver. (B) *In vivo* viral clearance, as determined by the presence of viral DNA in the livers of infected mice at 24 h and 28 days p.i. Total DNA was purified from liver fragments, and qPCR of viral DNA was performed, as described in Materials and Methods. Normalization with the cellular genomic standard (IFN-β) was used to derive the relative viral DNA yield/host genome. Data represent the averages of results from biological and technical triplicates. Nine mice were analyzed for each strain. nd, not determined. (C) Serum antiviral antibody activity, as determined by antibody-Ad5βGal neutralization assays in HeLa cells (see Materials and Methods). Three independent experiments were performed (*, $P < 0.05$ was considered significant).

low-level residual vDNA was detected at 4 weeks postinfection in all infected strains. Based on data from the β-Gal reporter assay, residual vDNA present at these later time points was not yielding detectable reporter gene expression. Clearance of the rAd5 vector from the liver is partly attributed to the development of antigen-specific cytotoxic T cells (49, 51, 61). Based on the data presented, impairment of the cGAS/STING antiviral recognition response does not compromise virus clearance from the liver.

Production of antiadenovirus neutralizing antibodies in cGAS/STING-deficient mice is minimally impacted. Adenovirus infections generate a potent neutralizing humoral immune response in the immunocompetent host. To assess the influence of cGAS/STING cascade mutants on the development of neutralizing antibody (NAb) against rAd5βGal, serum was harvested from mock- or rAd5βGal-infected mice at 28 days postinfection (n = 6/strain). A HeLa cell rAd5βGal transduction-blocking assay was used to assess NAb in serum samples from infected WT and knockout mice (as described in Materials and Methods) (Fig. 6C). Controls consisting of incubation of rAd5βGal with medium (no serum) or a 1:40 dilution of mock-treated WT serum resulted in similarly high levels of β-Gal expression. Sera from the infected WT strain and each cGAS/STING cascade-deficient strain at day 28 postinfection effectively blocked rAd5βGal transduction in a concentration-dependent manner. Although each strain developed NAbs against rAd5, higher luminescence levels in infected cGAS$^{-/-}$ serum suggest that the NAb titer produced by infection of cGAS$^{-/-}$ mice was slightly but significantly lower than the NAb titer generated from WT mice.

DISCUSSION

Induction of the type I interferon antiviral response is a well-established mechanism for controlling virus infections. For both RNA and DNA viruses, viral nucleic acids are key pathogen-associated molecular patterns recognized by host pattern recognition receptors in a cell-specific manner. An array of nucleic acid-sensing PRRs have been identified, which leads to IRF3 activation and the induction of the type I interferon antiviral response. We have asked how the cGAS/STING DNA-sensing cascade contributes to the antiadenovirus recognition response *in vitro* and *in vivo* in the nonpermissive mouse model. We have demonstrated that cGAS/STING-dependent signaling is essential for initiating an *in vitro* antiviral response in murine APCs following exposure to rAdV. Furthermore, the cGAS/STING DNA-sensing cascade has a major role in defining antiviral inflammatory responses *in vivo* at early times postinfection (5 h). The data also indicate that cGAS/STING-independent antiviral recognition pathways were activated following systemic administration of rAdV. In spite of compromised APC activation *in vitro* and early antiviral response deficiencies in cGAS/STING knockout mice, adaptive immune endpoint assays (vector clearance and neutralizing antibody at 28 days postinfection) were only marginally affected compared to those for wild-type mice. Based on the latter observations, we conclude that the cGAS/STING DNA-sensing cascade is not essential for clearance of infected cells or the generation of a humoral immune response to rAd vectors.

Criteria used to assess cGAS/STING-dependent antiviral responses in primary BMMOs and BMDCs included the activation of primary and secondary response markers (^{pSer172}TBK1, ^{pSer396}IRF3, and ^{pTyr701}STAT1), transcriptional induction of established antiviral and proinflammatory genes, and increased surface expression of CD86 costimulatory proteins. In BMMOs from

cGAS and STING knockout strains, the lack of a significant antiviral response indicates that the antiviral recognition/signaling response under these *in vitro* conditions is exclusively dependent on cGAS activation of the STING adaptor pathway. IRF3 knockout mice were used for comparison as a negative control. As the one established target of the cGAS/STING/TBK1 signaling cascade, the IRF3 knockout phenotype might be expected to be phenotypically similar to both cGAS and STING mutations. Data from *in vitro* assays of BMMO activation and maturation were completely in agreement with this premise, indicating that cGAS/STING/TBK1/IRF3 is the featured antiadenovirus recognition response pathway for BMMOs.

We came to a similar conclusion with BMDCs, but there were noticeable differences. The cGAS/STING cascade is required for primary and secondary signaling, transcript induction, and the upregulation of the maturation marker CD86. However, when rAdV induction of RNA transcripts from cGAS- and STING-deficient BMDCs was assessed, a low-level, cGAS/STING-independent, transcript-specific induction response was detected (Fig. 3B). This low-level response was not observed for IFN-β mRNA but was detected for select ISGs and proinflammatory transcripts. In BMDCs, we also found several features that distinguished the IRF3 knockout strain from both cGAS and STING knockout BMDCs. As noted above for BMMOs, levels of pTBK1 were induced by rAdV in IRF3$^{-/-}$ mouse-derived cells. Levels of pSTAT1 were also detectable at 6 h postinfection in IRF3$^{-/-}$ BMDCs but not in AdV-treated cGAS$^{-/-}$ or STING$^{-/-}$ cells. Furthermore, levels of transcript induction in IRF3$^{-/-}$ BMDC were significantly higher for IFN-β after infection and trending toward higher levels for viperin, proinflammatory transcripts, and ISGs than for cGAS$^{-/-}$ and STING$^{-/-}$ BMDC. One possible explanation for the low-level antiviral response in IRF3$^{-/-}$ BMDCs but not in cGAS$^{-/-}$ or STING$^{-/-}$ BMDCs would be TBK1 activation of a second IRF substrate that is not available to the same extent in BMMOs. IRF7 is the most obvious candidate (19), and a recent study indicated that a cGAS-independent STING/IRF7 pathway plays a significant role in the immune response to DNA vaccines (62). Other possibilities include secondary signaling targets of cGAMP or STING, independent of TBK1. Further studies will be required to determine the mechanism contributing to residual activity in the knockout BMDCs. These observations indicate that cell-specific phenotypes are detectable when cGAS and STING knockouts are compared to IRF3 knockouts. The virus recognition complexes operating in BMDCs indicate a greater degree of complexity than those functioning in BMMOs.

Specific explanations for differences between BMMOs and BMDCs could involve secondary PRRs functioning in BMDCs but not BMMOs. Such a BMDC pathway necessarily signals through a STING/TBK1/IRF3-independent mechanism. MyD88 signaling pathways that influence the APC response to rAdVs are one possibility; enhanced activities of IFI16, DDX41, or AIM2 are examples of established DNA sensors that may operate in BMDCs as secondary DNA sensors that are able to engage in STING-independent signaling. Alternatively, cell-specific differences in intracellular signaling through penton-integrin stimulation may differentially influence the induction of a subpopulation of antiviral/inflammatory transcripts following infection. Since secondary signaling by IFNs (pSTAT1) was not evident, and upregulation of the CD86 maturation marker was not observed, we believe that the low-level transcription response to rAdV in cGAS and STING knockout BMDCs is biased toward an NF-κB-dependent inflammatory response and not an IFN-inducing mechanism.

The early antiviral response to systemically administered rAdV in cGAS$^{-/-}$ and STING$^{-/-}$ mice compared to that in WT or IRF3$^{-/-}$ mice was largely consistent with the *in vitro* characterization of APCs. By using an ELISA to quantify serum levels of IFN-β at 5 h postinfection, significant induction was found for WT mice but was absent in STING$^{-/-}$ and cGAS$^{-/-}$ mice and marginally detectable in IRF3$^{-/-}$ mice. This observation was consistent with levels of total liver IFN-β mRNA expressed following virus infection. Inflammatory cytokines corresponding to TNF-α, IL-6, and IL-10 were induced in WT mice, and levels of induction were significantly lower in knockout strains. TNF-α and IL-6 transcript induction occurred in WT mice but was significantly reduced in each knockout strain. ISG transcript induction was predictably diminished in knockout strains. Because total liver RNA assays reflect a population of cell types, we believe that a major contributor to the induction profile arises from Kupffer cell uptake of adenovirus and secondary signaling events through the expression of IFNs. Systemic delivery of rAdV exposes the virus to serum factor binding as well as opsonization, which impacts virus uptake into a variety of cell types. This may expose the virus to PRRs other than cGAS. Our data indicate that following systemic administration of rAdV, signaling through the cGAS/STING cascade was the predominant mechanism for the induction of antiviral response transcripts.

Previous studies established that compromised dendritic cell activation/maturation (63) influenced both the clearance of infected cells and the induction of an antiviral humoral immune response. Although BMDC activation and maturation were compromised in cells derived from the cGAS$^{-/-}$, STING$^{-/-}$, or IRF3$^{-/-}$ strain, using systemically administered virus *in vivo*, both vector clearance and antiviral neutralizing antibody responses occurred. The minimal impact of the type I IFN antiviral response on the adaptive immune response to AdV is consistent with data from studies characterizing antiadenovirus responses in the STAT2 knockout Syrian hamster model (64) and recent observations of rAdV vaccine vectors in IFNRI and STING knockout strains (65). Our observations that compromised dendritic cell maturation *in vitro* can be separated from an adaptive immune response phenotype are consistent with the characterization of the antiviral response to rAdV in type I IFN receptor knockout mice (66).

The cGAS/STING cascade has been viewed as an adjuvant target for vaccine applications (20). Clearly, this pathway facilitates APC presentation and upregulation of costimulatory molecules. Our observation that the anti-Ad neutralizing antibody level was modestly reduced in cGAS-deficient mice is consistent with such a role. The distinct parameters necessary for triggering an adaptive immune response through dendritic cell migration/activation and those required for the adjuvant properties associated with stimulation of the cGAS/STING cascade require further investigation. *In vivo*, DC maturation and migration following virus activation are complex and dynamic processes leading to CD4 and CD8 T-cell priming. Recent reports have revealed that for different viruses, infection and DC migration to lymph nodes result in distinct spatially and temporally defined interactions between CD4 and CD8 T cells and multiple subsets of DCs (67, 68). The factors that influence these distinct DC interactions with T-cell subsets have not been fully established for Ad infections. The residual low-level antiadenovirus activation response identified following infection of cGAS/STING-deficient BMDCs may be augmented

by unidentified *in vivo* interactions leading to eventual T- and B-cell priming in regional lymph nodes. Further studies will be required to identify these interactions. The studies presented here have established the cGAS/STING pathway as the dominant antiadenovirus type I IFN-inducing cascade *in vitro* and *in vivo* in the murine model, with no observed impact on viral clearance, and a cGAS deficiency resulted in a slightly diminished humoral immune response to viral infection.

ACKNOWLEDGMENTS

We thank Donna MacDuff (Washington University) for her help in establishing and screening the cGAS$^{-/-}$ C57BL/6 mouse strain. We thank Yuan-Shan Zhu, Francisco G. Santiago, and the Weill Cornell Medicine CTSC core facility for technical assistance.

FUNDING INFORMATION

This work, including the efforts of Erik Falck-Pedersen, was funded by HHS | NIH | National Institute of Allergy and Infectious Diseases (NIAID) (AI094050). This work, including the efforts of Erik Falck-Pedersen, was funded by Hearst Foundation.

REFERENCES

1. **Lynch JP, III, Fishbein M, Echavarria M.** 2011. Adenovirus. Semin Respir Crit Care Med **32:**494–511. http://dx.doi.org/10.1055/s-0031-1283287.
2. **Wolff G, Worgall S, van Rooijen N, Song WR, Harvey BG, Crystal RG.** 1997. Enhancement of in vivo adenovirus-mediated gene transfer and expression by prior depletion of tissue macrophages in the target organ. J Virol **71:**624–629.
3. **Xu Z, Tian J, Smith JS, Byrnes AP.** 2008. Clearance of adenovirus by Kupffer cells is mediated by scavenger receptors, natural antibodies, and complement. J Virol **82:**11705–11713. http://dx.doi.org/10.1128/JVI.01320-08.
4. **Khare R, Hillestad ML, Xu Z, Byrnes AP, Barry MA.** 2013. Circulating antibodies and macrophages as modulators of adenovirus pharmacology. J Virol **87:**3678–3686. http://dx.doi.org/10.1128/JVI.01392-12.
5. **Cerullo V, Seiler MP, Mane V, Brunetti-Pierri N, Clarke C, Bertin TK, Rodgers JR, Lee B.** 2007. Toll-like receptor 9 triggers an innate immune response to helper-dependent adenoviral vectors. Mol Ther **15:**378–385. http://dx.doi.org/10.1038/sj.mt.6300031.
6. **Nociari M, Ocheretina O, Schoggins JW, Falck-Pedersen E.** 2007. Sensing infection by adenovirus: Toll-like receptor-independent viral DNA recognition signals activation of the interferon regulatory factor 3 master regulator. J Virol **81:**4145–4157. http://dx.doi.org/10.1128/JVI.02685-06.
7. **Zhu J, Huang X, Yang Y.** 2007. Innate immune response to adenoviral vectors is mediated by both Toll-like receptor-dependent and -independent pathways. J Virol **81:**3170–3180. http://dx.doi.org/10.1128/JVI.02192-06.
8. **Muruve DA, Petrilli V, Zaiss AK, White LR, Clark SA, Ross PJ, Parks RJ, Tschopp J.** 2008. The inflammasome recognizes cytosolic microbial and host DNA and triggers an innate immune response. Nature **452:**103–107. http://dx.doi.org/10.1038/nature06664.
9. **Di Paolo NC, Miao EA, Iwakura Y, Murali-Krishna K, Aderem A, Flavell RA, Papayannopoulou T, Shayakhmetov DM.** 2009. Virus binding to a plasma membrane receptor triggers interleukin-1 alpha-mediated proinflammatory macrophage response in vivo. Immunity **31:**110–121. http://dx.doi.org/10.1016/j.immuni.2009.04.015.
10. **Beladi I, Pusztai R.** 1967. Interferon-like substance produced in chick fibroblast cells inoculated with human adenoviruses. Z Naturforsch B **22:**165–169.
11. **Ho M, Kohler K.** 1967. Studies on human adenoviruses as inducers of interferon in chick cells. Arch Gesamte Virusforsch **22:**69–78. http://dx.doi.org/10.1007/BF01240504.
12. **Toth M, Bakay M, Tarodi B, Toth S, Pusztai R, Beladi I.** 1983. Different interferon-inducing ability of human adenovirus types in chick embryo cells. Acta Virol **27:**337–345.
13. **Kawai T, Akira S.** 2007. Antiviral signaling through pattern recognition receptors. J Biochem **141:**137–145.
14. **Thompson MR, Kaminski JJ, Kurt-Jones EA, Fitzgerald KA.** 2011. Pattern recognition receptors and the innate immune response to viral infection. Viruses **3:**920–940. http://dx.doi.org/10.3390/v3060920.
15. **Unterholzner L.** 2013. The interferon response to intracellular DNA: why so many receptors? Immunobiology **218:**1312–1321. http://dx.doi.org/10.1016/j.imbio.2013.07.007.
16. **Kawai T, Sato S, Ishii KJ, Coban C, Hemmi H, Yamamoto M, Terai K, Matsuda M, Inoue J, Uematsu S, Takeuchi O, Akira S.** 2004. Interferon-alpha induction through Toll-like receptors involves a direct interaction of IRF7 with MyD88 and TRAF6. Nat Immunol **5:**1061–1068. http://dx.doi.org/10.1038/ni1118.
17. **Honda K, Yanai H, Negishi H, Asagiri M, Sato M, Mizutani T, Shimada N, Ohba Y, Takaoka A, Yoshida N, Taniguchi T.** 2005. IRF-7 is the master regulator of type-I interferon-dependent immune responses. Nature **434:**772–777. http://dx.doi.org/10.1038/nature03464.
18. **Ning S, Pagano JS, Barber GN.** 2011. IRF7: activation, regulation, modification and function. Genes Immun **12:**399–414. http://dx.doi.org/10.1038/gene.2011.21.
19. **Fejer G, Drechsel L, Liese J, Schleicher U, Ruzsics Z, Imelli N, Greber UF, Keck S, Hildenbrand B, Krug A, Bogdan C, Freudenberg MA.** 2008. Key role of splenic myeloid DCs in the IFN-alphabeta response to adenoviruses in vivo. PLoS Pathog **4:**e1000208. http://dx.doi.org/10.1371/journal.ppat.1000208.
20. **Li XD, Wu J, Gao D, Wang H, Sun L, Chen ZJ.** 29 August 2013. Pivotal roles of cGAS-cGAMP signaling in antiviral defense and immune adjuvant effects. Science http://dx.doi.org/10.1126/science.1244040.
21. **Sun L, Wu J, Du F, Chen X, Chen ZJ.** 2013. Cyclic GMP-AMP synthase is a cytosolic DNA sensor that activates the type I interferon pathway. Science **339:**786–791. http://dx.doi.org/10.1126/science.1232458.
22. **Lam E, Falck-Pedersen E.** 2014. Unabated adenovirus replication following activation of the cGAS/STING-dependent antiviral response in human cells. J Virol **88:**14426–14439. http://dx.doi.org/10.1128/JVI.02608-14.
23. **Lam E, Stein S, Falck-Pedersen E.** 2014. Adenovirus detection by the cGAS/STING/TBK1 DNA sensing cascade. J Virol **88:**974–981. http://dx.doi.org/10.1128/JVI.02702-13.
24. **Civril F, Deimling T, de Oliveira Mann CC, Ablasser A, Moldt M, Witte G, Hornung V, Hopfner KP.** 2013. Structural mechanism of cytosolic DNA sensing by cGAS. Nature **498:**332–337. http://dx.doi.org/10.1038/nature12305.
25. **Zhang X, Wu J, Du F, Xu H, Sun L, Chen Z, Brautigam CA, Zhang X, Chen ZJ.** 2014. The cytosolic DNA sensor cGAS forms an oligomeric complex with DNA and undergoes switch-like conformational changes in the activation loop. Cell Rep **6:**421–430. http://dx.doi.org/10.1016/j.celrep.2014.01.003.
26. **Diner EJ, Burdette DL, Wilson SC, Monroe KM, Kellenberger CA, Hyodo M, Hayakawa Y, Hammond MC, Vance RE.** 2013. The innate immune DNA sensor cGAS produces a noncanonical cyclic dinucleotide that activates human STING. Cell Rep **3:**1355–1361. http://dx.doi.org/10.1016/j.celrep.2013.05.009.
27. **Gao P, Ascano M, Wu Y, Barchet W, Gaffney BL, Zillinger T, Serganov AA, Liu Y, Jones RA, Hartmann G, Tuschl T, Patel DJ.** 2013. Cyclic [G(2′,5′)pA(3′,5′)p] is the metazoan second messenger produced by DNA-activated cyclic GMP-AMP synthase. Cell **153:**1094–1107. http://dx.doi.org/10.1016/j.cell.2013.04.046.
28. **Saitoh T, Fujita N, Hayashi T, Takahara K, Satoh T, Lee H, Matsunaga K, Kageyama S, Omori H, Noda T, Yamamoto N, Kawai T, Ishii K, Takeuchi O, Yoshimori T, Akira S.** 2009. Atg9a controls dsDNA-driven dynamic translocation of STING and the innate immune response. Proc Natl Acad Sci U S A **106:**20842–20846. http://dx.doi.org/10.1073/pnas.0911267106.
29. **Konno H, Konno K, Barber GN.** 2013. Cyclic dinucleotides trigger ULK1 (ATG1) phosphorylation of STING to prevent sustained innate immune signaling. Cell **155:**688–698. http://dx.doi.org/10.1016/j.cell.2013.09.049.
30. **Ishikawa H, Ma Z, Barber GN.** 2009. STING regulates intracellular DNA-mediated, type I interferon-dependent innate immunity. Nature **461:**788–792. http://dx.doi.org/10.1038/nature08476.
31. **Tanaka Y, Chen ZJ.** 2012. STING specifies IRF3 phosphorylation by TBK1 in the cytosolic DNA signaling pathway. Sci Signal **5:**ra20. http://dx.doi.org/10.1126/scisignal.2002521.
32. **Wang Q, Liu X, Cui Y, Tang Y, Chen W, Li S, Yu H, Pan Y, Wang C.** 2014. The E3 ubiquitin ligase AMFR and INSIG1 bridge the activation of TBK1 kinase by modifying the adaptor STING. Immunity **41:**919–933. http://dx.doi.org/10.1016/j.immuni.2014.11.011.

33. **Wathelet MG, Lin CH, Parekh BS, Ronco LV, Howley PM, Maniatis T.** 1998. Virus infection induces the assembly of coordinately activated transcription factors on the IFN-beta enhancer in vivo. Mol Cell **1:**507–518. http://dx.doi.org/10.1016/S1097-2765(00)80051-9.
34. **Hiscott J, Pitha P, Genin P, Nguyen H, Heylbroeck C, Mamane Y, Algarte M, Lin R.** 1999. Triggering the interferon response: the role of IRF-3 transcription factor. J Interferon Cytokine Res **19:**1–13. http://dx.doi.org/10.1089/107999099314360.
35. **Agalioti T, Lomvardas S, Parekh B, Yie J, Maniatis T, Thanos D.** 2000. Ordered recruitment of chromatin modifying and general transcription factors to the IFN-beta promoter. Cell **103:**667–678. http://dx.doi.org/10.1016/S0092-8674(00)00169-0.
36. **Panne D, Maniatis T, Harrison SC.** 2004. Crystal structure of ATF-2/c-Jun and IRF-3 bound to the interferon-beta enhancer. EMBO J **23:**4384–4393. http://dx.doi.org/10.1038/sj.emboj.7600453.
37. **Stein SC, Lam E, Falck-Pedersen E.** 2012. Cell-specific regulation of nucleic acid sensor cascades: a controlling interest in the antiviral response. J Virol **86:**13303–13312. http://dx.doi.org/10.1128/JVI.02296-12.
38. **Haque SJ, Williams BR.** 1998. Signal transduction in the interferon system. Semin Oncol **25:**14–22.
39. **Qureshi SA, Salditt-Georgieff M, Darnell JE, Jr.** 1995. Tyrosine-phosphorylated Stat1 and Stat2 plus a 48-kDa protein all contact DNA in forming interferon-stimulated-gene factor 3. Proc Natl Acad Sci U S A **92:**3829–3833. http://dx.doi.org/10.1073/pnas.92.9.3829.
40. **Shayakhmetov DM, Gaggar A, Ni S, Li ZY, Lieber A.** 2005. Adenovirus binding to blood factors results in liver cell infection and hepatotoxicity. J Virol **79:**7478–7491. http://dx.doi.org/10.1128/JVI.79.12.7478-7491.2005.
41. **Kalyuzhniy O, Di Paolo NC, Silvestry M, Hofherr SE, Barry MA, Stewart PL, Shayakhmetov DM.** 2008. Adenovirus serotype 5 hexon is critical for virus infection of hepatocytes in vivo. Proc Natl Acad Sci U S A **105:**5483–5488. http://dx.doi.org/10.1073/pnas.0711757105.
42. **Waddington SN, McVey JH, Bhella D, Parker AL, Barker K, Atoda H, Pink R, Buckley SM, Greig JA, Denby L, Custers J, Morita T, Francischetti IM, Monteiro RQ, Barouch DH, van Rooijen N, Napoli C, Havenga MJ, Nicklin SA, Baker AH.** 2008. Adenovirus serotype 5 hexon mediates liver gene transfer. Cell **132:**397–409. http://dx.doi.org/10.1016/j.cell.2008.01.016.
43. **Alba R, Bradshaw AC, Parker AL, Bhella D, Waddington SN, Nicklin SA, van Rooijen N, Custers J, Goudsmit J, Barouch DH, McVey JH, Baker AH.** 2009. Identification of coagulation factor (F)X binding sites on the adenovirus serotype 5 hexon: effect of mutagenesis on FX interactions and gene transfer. Blood **114:**965–971. http://dx.doi.org/10.1182/blood-2009-03-208835.
44. **Qiu Q, Xu Z, Tian J, Moitra R, Gunti S, Notkins AL, Byrnes AP.** 31 December 2014. Impact of natural IgM concentration on gene therapy with adenovirus type 5 vectors. J Virol http://dx.doi.org/10.1128/JVI.03217-14.
45. **Zaiss AK, Vilaysane A, Cotter MJ, Clark SA, Meijndert HC, Colarusso P, Yates RM, Petrilli V, Tschopp J, Muruve DA.** 2009. Antiviral antibodies target adenovirus to phagolysosomes and amplify the innate immune response. J Immunol **182:**7058–7068. http://dx.doi.org/10.4049/jimmunol.0804269.
46. **Muruve DA, Barnes MJ, Stillman IE, Libermann TA.** 1999. Adenoviral gene therapy leads to rapid induction of multiple chemokines and acute neutrophil-dependent hepatic injury in vivo. Hum Gene Ther **10:**965–976. http://dx.doi.org/10.1089/10430349950018364.
47. **Worgall S, Wolff G, Falck-Pedersen E, Crystal RG.** 1997. Innate immune mechanisms dominate elimination of adenoviral vectors following in vivo administration. Hum Gene Ther **8:**37–44. http://dx.doi.org/10.1089/hum.1997.8.1-37.
48. **Banchereau J, Steinman RM.** 1998. Dendritic cells and the control of immunity. Nature **392:**245–252. http://dx.doi.org/10.1038/32588.
49. **Yang Y, Ertl HC, Wilson JM.** 1994. MHC class I-restricted cytotoxic T lymphocytes to viral antigens destroy hepatocytes in mice infected with E1-deleted recombinant adenoviruses. Immunity **1:**433–442. http://dx.doi.org/10.1016/1074-7613(94)90074-4.
50. **Yang Y, Li Q, Ertl HC, Wilson JM.** 1995. Cellular and humoral immune responses to viral antigens create barriers to lung-directed gene therapy with recombinant adenoviruses. J Virol **69:**2004–2015.
51. **Yang Y, Wilson JM.** 1995. Clearance of adenovirus-infected hepatocytes by MHC class I-restricted CD4+ CTLs in vivo. J Immunol **155:**2564–2570.
52. **Schoggins JW, Falck-Pedersen E.** 2006. Fiber and penton base capsid modifications yield diminished adenovirus type 5 transduction and proinflammatory gene expression with retention of antigen-specific humoral immunity. J Virol **80:**10634–10644. http://dx.doi.org/10.1128/JVI.01359-06.
53. **Philpott NJ, Nociari M, Elkon KB, Falck-Pedersen E.** 2004. Adenovirus-induced maturation of dendritic cells through a PI3 kinase-mediated TNF-alpha induction pathway. Proc Natl Acad Sci U S A **101:**6200–6205. http://dx.doi.org/10.1073/pnas.0308368101.
54. **Lutz MB, Kukutsch N, Ogilvie AL, Rossner S, Koch F, Romani N, Schuler G.** 1999. An advanced culture method for generating large quantities of highly pure dendritic cells from mouse bone marrow. J Immunol Methods **223:**77–92. http://dx.doi.org/10.1016/S0022-1759(98)00204-X.
55. **Schmittgen TD, Livak KJ.** 2008. Analyzing real-time PCR data by the comparative C(T) method. Nat Protoc **3:**1101–1108. http://dx.doi.org/10.1038/nprot.2008.73.
56. **Livak KJ, Schmittgen TD.** 2001. Analysis of relative gene expression data using real-time quantitative PCR and the 2(-Delta Delta C(T)) method. Methods **25:**402–408. http://dx.doi.org/10.1006/meth.2001.1262.
57. **Miller SA, Dykes DD, Polesky HF.** 1988. A simple salting out procedure for extracting DNA from human nucleated cells. Nucleic Acids Res **16:**1215. http://dx.doi.org/10.1093/nar/16.3.1215.
58. **Bradford MM.** 1976. A rapid and sensitive method for the quantitation of microgram quantities of protein utilizing the principle of protein-dye binding. Anal Biochem **72:**248–254. http://dx.doi.org/10.1016/0003-2697(76)90527-3.
59. **Sauer JD, Sotelo-Troha K, von Moltke J, Monroe KM, Rae CS, Brubaker SW, Hyodo M, Hayakawa Y, Woodward JJ, Portnoy DA, Vance RE.** 2011. The N-ethyl-N-nitrosourea-induced Goldenticket mouse mutant reveals an essential function of Sting in the in vivo interferon response to Listeria monocytogenes and cyclic dinucleotides. Infect Immun **79:**688–694. http://dx.doi.org/10.1128/IAI.00999-10.
60. **Schoggins JW, MacDuff DA, Imanaka N, Gainey MD, Shrestha B, Eitson JL, Mar KB, Richardson RB, Ratushny AV, Litvak V, Dabelic R, Manicassamy B, Aitchison JD, Aderem A, Elliott RM, Garcia-Sastre A, Racaniello V, Snijder EJ, Yokoyama WM, Diamond MS, Virgin HW, Rice CM.** 2014. Pan-viral specificity of IFN-induced genes reveals new roles for cGAS in innate immunity. Nature **505:**691–695. http://dx.doi.org/10.1038/nature12862.
61. **Yang Y, Nunes FA, Berencsi K, Furth EE, Gonczol E, Wilson JM.** 1994. Cellular immunity to viral antigens limits E1-deleted adenoviruses for gene therapy. Proc Natl Acad Sci U S A **91:**4407–4411. http://dx.doi.org/10.1073/pnas.91.10.4407.
62. **Suschak JJ, Wang S, Fitzgerald KA, Lu S.** 2016. A cGAS-independent STING/IRF7 pathway mediates the immunogenicity of DNA vaccines. J Immunol **196:**310–316. http://dx.doi.org/10.4049/jimmunol.1501836.
63. **Trevejo JM, Marino MW, Philpott N, Josien R, Richards EC, Elkon KB, Falck-Pedersen E.** 2001. TNF-alpha-dependent maturation of local dendritic cells is critical for activating the adaptive immune response to virus infection. Proc Natl Acad Sci U S A **98:**12162–12167. http://dx.doi.org/10.1073/pnas.211423598.
64. **Toth K, Lee SR, Ying B, Spencer JF, Tollefson AE, Sagartz JE, Kong IK, Wang Z, Wold WS.** 2015. STAT2 knockout Syrian hamsters support enhanced replication and pathogenicity of human adenovirus, revealing an important role of type I interferon response in viral control. PLoS Pathog **11:**e1005084. http://dx.doi.org/10.1371/journal.ppat.1005084.
65. **Quinn KM, Zak DE, Costa A, Yamamoto A, Kastenmuller K, Hill BJ, Lynn GM, Darrah PA, Lindsay RW, Wang L, Cheng C, Nicosia A, Folgori A, Colloca S, Cortese R, Gostick E, Price DA, Gall JG, Roederer M, Aderem A, Seder RA.** 2015. Antigen expression determines adenoviral vaccine potency independent of IFN and STING signaling. J Clin Invest **125:**1129–1146. http://dx.doi.org/10.1172/JCI78280.
66. **Hensley SE, Giles-Davis W, McCoy KC, Weninger W, Ertl HC.** 2005. Dendritic cell maturation, but not CD8+ T cell induction, is dependent on type I IFN signaling during vaccination with adenovirus vectors. J Immunol **175:**6032–6041. http://dx.doi.org/10.4049/jimmunol.175.9.6032.
67. **Eickhoff S, Brewitz A, Gerner MY, Klauschen F, Komander K, Hemmi H, Garbi N, Kaisho T, Germain RN, Kastenmuller W.** 2015. Robust anti-viral immunity requires multiple distinct T cell-dendritic cell interactions. Cell **162:**1322–1337. http://dx.doi.org/10.1016/j.cell.2015.08.004.
68. **Hor JL, Whitney PG, Zaid A, Brooks AG, Heath WR, Mueller SN.** 2015. Spatiotemporally distinct interactions with dendritic cell subsets facilitates CD4+ and CD8+ T cell activation to localized viral infection. Immunity **43:**554–565. http://dx.doi.org/10.1016/j.immuni.2015.07.020.